Haneda, Katsuyuki; Nguyen, Sinh Le Hong; Khatun, Afroza

Attainable capacity of spatial radio channels

Published in:
2016 IEEE Globecom Workshops, GC Wkshps 2016 - Proceedings

DOI:
10.1109/GLOCOMW.2016.7848843

Published: 08/12/2016

Document Version
Peer-reviewed accepted author manuscript, also known as Final accepted manuscript or Post-print

Please cite the original version:
Haneda, K., Nguyen, S. L. H., & Khatun, A. (2016). Attainable capacity of spatial radio channels: A multiple-frequency analysis. In *2016 IEEE Globecom Workshops, GC Wkshps 2016 - Proceedings* Article 7848843 (IEEE Globecom Workshops). IEEE. https://doi.org/10.1109/GLOCOMW.2016.7848843

Attainable Capacity of Spatial Radio Channels: A Multiple-Frequency Analysis

Katsuyuki Haneda*, Sinh Le Hong Nguyen* and Afroza Khatun*
*Aalto University School of Electrical Engineering
Espoo, Finland FI00076-AALTO, Email: katsuyuki.haneda@aalto.fi

***Abstract*—This paper reports an attainable channel capacity and spatial degrees-of-freedom of multiple-antenna radio channels at 15, 28 and 61 GHz. The analysis is based on channel sounding in a same street canyon. The attainable capacity is evaluated so that it depends only on the antenna aperture size but is independent of implementation of antenna elements on the aperture. The analysis shows that multipath richness decreases as the frequency increases, as indicated by the smaller spatial degrees-of-freedom at higher frequencies for the same electrical aperture size of the receive antenna. The analysis furthermore reveals that channels at the three radio frequencies can attain almost the same level of capacity for a given transmit power and physical size of the receive antenna. The result is explained by a greater electrical size of the antenna aperture at the higher frequencies that can leverage higher gains and finer angular resolution and hence normalize the availability of fewer multipaths.**

I. Introduction

Demands of very high data rate radio communications are ever increasing in the cellular context, for which a novel physical layer technology is required. The use of higher frequencies than 6 GHz up to millimeter-wave band is among possible candidate methods to fulfill the demand. One of the important open questions in cellular system design exploiting the higher frequency bands is the choice of the radio frequency that provides sufficiently high channel capacity. In addition to the available bandwidth defined by the spectrum regulation, the physical radio channels also determine the attainable channel capacity at a specific frequency band. For example, it has been known for many years that radio systems operating at higher frequencies than 6 GHz can offer the same or even better link budget as low frequency systems with the same antenna aperture size for a line-of-sight (LOS) scenario [1]. This is attributed to the greater electrical size of an antenna aperture of a fixed physical size as the frequency goes higher, leading to higher beam focusing gain that compensates for the pathloss. On the other hand, the frequency dependency of radio channels is non-trivial when it comes to *spatial multipath richness*. The multipath richness is of particular relevance to the high frequency because of their potential of spatial data and user multiplexing per time-frequency resource. The radio propagation below 6 GHz provides rich multipaths due to abundant reflection and scattering from the surrounding environment, while antenna aperture equipped in a communication device may not be electrically large enough for significant spatial multiplexing; in this case, the advantage of rich multipath propagation may not be fully exploited by the antenna aperture. On the other hand, millimeter-wave frequency band, e.g., 60 GHz, offers electrically large antenna even with a physically small aperture to steer narrow beams towards users and allows much better spatial multiplexing capability. In contrast, there are fewer multipaths in radio wave propagation due to angularly-selective reflection, diffraction and scattering that may limit the spatial multiplexing. Here advantage of the large antenna aperture size may not be fully exploited due to the multipath sparsity in the radio propagation. It is therefore possible that multiple-antenna radio systems operate optimally at a radio frequency whereby they take full advantage of both the multipath richness and large-enough antenna aperture for improving the spectral efficiency. Comparisons of the attainable channel capacity of multiple antenna channels at different radio frequencies are therefore the goal of this paper.

Previous studies shed lights on frequency dependency of multipath richness for capacity improvement only to a limited extent; the work [2] compares the capacity in an urban scenario at 28 and 73 GHz, showing that they provide almost the same channel capacity. While the work [3] infers from a single indoor channel analysis that 5 GHz radio frequency may provide the best channel capacity. It is apparent that there are much more rooms to be studied such that wider radio frequency ranges and more radio environments are covered. This paper adds insights into the attainable capacity of multiple-antenna channels at 15, 28 and 61 GHz through channel sounding in a same urban street canyon [4]. The attainable capacity is analyzed by defining the spatial channels with respect to the *modes* of antenna *aperture*, e.g., [3], [5], [6], and not to the antenna *elements* as traditionally done. We show from the analysis that the attainable capacity can be almost comparable at the three frequencies, which supports the finding in [2], though there are exceptions depending on propagation conditions.

In the remainder of the paper, we introduce the definition of the spatial channel and its attainable capacity in Section II. Section III provides the multi-frequency channel sounding in a campus street canyon at 15, 28 and 61 GHz. Having compared the attainable capacity at the three frequencies in Section IV, we summarize our findings in Section V.

II. Spatial Channels, Their Degrees-of-Freedom and Attainable Capacity

The capacity of multiple-antenna channels depends on the multipath richness and the antenna array configuration. In

order to make the analysis generic and applicable to *any* possible antenna array configurations, we evaluate the attainable capacity of radio channels with certain antenna *aperture*. A physical area where the antenna array is implemented is called aperture. A rule of thumb shows that antenna aperture that can be enclosed by a sphere of the minimum radius r_0 supports up to J spherical *modes* given by

$$J = 2N(N+2), \quad N = \lfloor k_0 r_0 \rfloor + \epsilon, \tag{1}$$

where k_0 is a wavenumber in the free space, $\lfloor \cdot \rfloor$ is the floor function, and ϵ is an uncertainty factor taking values between 0 and 10 for practical antennas [7]. The underlying physics behind (1) is that an electromagnetic field modeled by modes higher than J attenuates rapidly from the antenna and does not propagate effectively over the free space. According to (1), larger antennas can support more modes to propagate over the channel.

Next we define the multipath channel in a similar way as [5]. The narrowband multipath channel is usually described by a set of propagation paths based on a plane wave assumption as

$$\mathcal{P}_\mathrm{p} = \{\boldsymbol{\alpha}_l, \boldsymbol{\Gamma}'_l\}_{l=1}^{L}, \tag{2}$$

where $\boldsymbol{\alpha} \in \mathbb{C}^{2\times 2}$ is a polarimetric complex amplitude, $\boldsymbol{\Gamma}' = [\phi' \ \theta']$ is a vector composed of azimuth and polar angles on the receive (Rx) side; this report considers a single-directional, i.e., single-input multiple-output, channels for simplicity. The notation $\boldsymbol{\alpha}_l$ means that a parameter value $\boldsymbol{\alpha}$ for the l-th propagation path, $1 \leq l \leq L$. The same channel can be expressed by a mode coupling vector between the transmit (Tx) and the Rx sides as

$$\boldsymbol{m} = \sum_{l=1}^{L} \boldsymbol{G}^T(\boldsymbol{\Gamma}'_l)\boldsymbol{\alpha}_l \boldsymbol{F}, \tag{3}$$

where $\boldsymbol{G}(\boldsymbol{\Gamma}') \in \mathbb{C}^{2\times J}$ and $\boldsymbol{F}$ denote the far-field electric field intensity of the Rx and Tx modes and $\cdot^T$ is a transpose operation of a matrix or a vector. In a three-dimensional case, the mode is defined by the orthonormal *spherical harmonics* [7]. Since we assume that the Tx antenna is an isotropic point source, the Tx far-field coefficient vector becomes $\boldsymbol{F} = [1 \ 1]^T$. The size of the column vector $\boldsymbol{m} \in \mathbb{C}^J$ is therefore determined by the Rx antenna aperture size given by (1).

Finally, capacity of the radio channel is derived from the mode coupling vector $\boldsymbol{m}$. A channel covariance matrix at the Rx is given by

$$\boldsymbol{R} = E_{\boldsymbol{m}}\left[\boldsymbol{m}\boldsymbol{m}^H\right], \tag{4}$$

where $E_{\boldsymbol{m}}[\cdot]$ refers to an ensemble average over realizations of $\boldsymbol{m}$ subject to the small-scale fading and $\cdot^H$ is a Hermitian transpose operation of a matrix or a vector. Denoting the eigenvalue decomposition of the covariance matrices as $\boldsymbol{R} = \boldsymbol{U}^H \boldsymbol{\Lambda} \boldsymbol{U}$ where $\boldsymbol{U}$ is a unitary matrix consisting of eigenvectors and $\boldsymbol{\Lambda}$ is a diagonal matrix composed of eigenvalues, the capacity is given by

$$C = \log_2\left(1 + \frac{P_\mathrm{t}}{\sigma^2}\mathrm{tr}(\boldsymbol{\Lambda})\right) \tag{5}$$

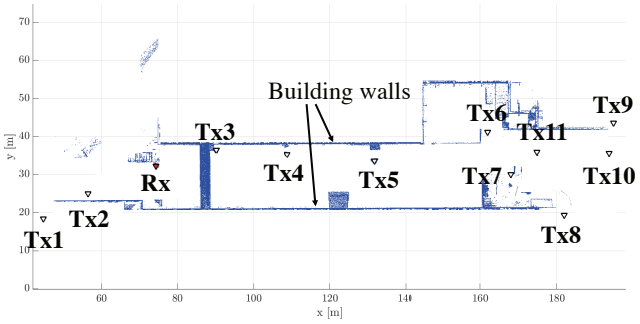

Fig. 1. Two-dimensional view of the measurement site, along with the Tx and Rx positions.

where σ^2 is noise variance at the Rx, P_t is a power to the Tx isotropic point source and $\mathrm{tr}(\cdot)$ is a trace of a matrix. The formula (5) gives a capacity that Rx antenna aperture of a specific size can achieve in multipath channels, and is called an intrinsic channel capacity [6]. Furthermore, the spatial degrees-of-freedom (SDoF) of the channel is estimated as

$$\mathrm{SDoF} = \arg\max_j \left(\frac{P_\mathrm{t}}{\sigma^2}\mathrm{diag}(\boldsymbol{\Lambda})_j \geq 1\right), \tag{6}$$

where $\mathrm{diag}(\boldsymbol{\Lambda})_j$ is a j-th diagonal element of a matrix $\boldsymbol{\Lambda}$. It is also assumed that the eigenvalues are sorted in the descending order, i.e., $\mathrm{diag}(\boldsymbol{\Lambda})_j \geq \mathrm{diag}(\boldsymbol{\Lambda})_{j+1}$ for $1 \leq j \leq J-1$. It is shown in [8] that (6) is an upper bound of the number of independent branches in spatial diversity channels.

III. Multiple-Frequency Channel Sounding

A. Channel Sounder

The multiple-frequency channel sounder operating at 15, 28 and 61 GHz is based on a vector network analyzer (VNA) that allows phase-synchronized measurements of scattering parameters with the radio channels being device-under-test. Channel measurements at 28 and 61 GHz are realized by mixing the VNA signals with local oscillator signals in frequency up- and down-converters, while there is no converters needed at 15 GHz. The VNA is capable of very wide-bandwidth measurements, but the measurement bandwidth is practically limited by the radio license. To allow measurements of long link distances, the sounder is equipped with 1) optical fiber cables to replace lossy coaxial cables at the frequency bands and 2) a high gain and directive horn antenna at the Rx side to increase the measurement dynamic range. In our channel sounder, the horn antennas at the three frequencies have almost identical electrical aperture size and hence the radiation patterns, allowing consistent angular resolutions at the three frequencies. We furthermore use two horn antennas for vertical and horizontal polarizations that have almost identical radiation patterns. Details of the channel sounder are described in [4].

B. Channel Sounding

We performed multi-frequency channel sounding in a campus street canyon scenario in Aalto University, Finland. The

two-dimensional view of the measurement site is shown in Fig. 1. The Rx antenna was fixed next to a shed at one side of the street, while the Tx antenna was placed at 11 different locations; the LOS locations were the same street as the Rx, whereas non-LOS (NLOS) locations were behind a corner at the end of the street canyon. It must be noted that the channel sounding at three frequencies was *not* performed at the same time, but with some time interval between sounding at different frequencies. Specifically, 15, 28 and 61 GHz measurements were performed in July, June and November 2015. This makes the channel at three frequencies not fully consistent to each other because of some moving objects such as cars parking on the street. For example, there were almost no parking cars at 28 GHz measurements, while the two sides of the street were occupied by parking cars during 15 and 61 GHz measurements. Since both the Tx and Rx antenna heights were above the rooftop of most cars and hence they do not shadow propagation paths off from side building walls if the Tx-Rx link distance is less than 80 m, i.e., to the left of Tx7 in Fig. 1. However, the Tx-Rx links with larger separation distances may have propagation paths shadowed by car roofs due to a slight slope of the street toward its end section [4]. In addition to cars, tree leaves are also significantly different for seasons, though its effect is expected to be limited in our measurement because only minor vegetation exists on one side of the street canyon.

For each Tx-Rx link, the horn antenna on the Rx side was scanned over the azimuth angles with 5° steps. The polar angle was set to 90°, i.e., the horizontal direction. The measurement was repeated with horn antennas having vertical and horizontal polarizations to obtain vertical-Tx/vertical-Rx and vertical-Tx/horizontal-Rx polarization measurements. A back-to-back (B2B) calibration was performed prior to the measurement by connecting interfaces of Tx and Rx antennas through a 20-dB attenuator. The calibration makes the measured channels represent characteristics of the antennas and radio wave propagation.

C. Channel Modeling

Propagation paths were detected from the measured power angular and delay profiles (PADPs). Exemplary PADPs from measurements at Tx3 are shown in Fig. 2. The figures include detected propagation paths indicated as crosses. The propagation paths were detected using a simple peak search method detailed in [9]. Each propagation path is characterized by a polarimetric path amplitude $\boldsymbol{\alpha}$, propagation delay time τ and azimuth angle of arrival ϕ', which compose the plane wave parameters defined in (2); the propagation delay estimates are not used for the link simulations. The polar angle θ' was set to 90° because the channel sounding did not perform antenna scanning over the polar angle, and subsequently, we assume that all the paths come from the horizontal directions[1]. The PADPs were derived with 500 MHz bandwidth at the three carrier frequencies to ensure the same angular-delay resolution of the propagation paths. The figures shows that dynamic range of the measurements differ noticeably; in concrete, they are 116.7, 127.9 and 145.7 dB at 15, 28 and 61 GHz, respectively, due to varying noise floor levels.

[1]It is not possible to analyze the effect of vertical dimension of antenna aperture on the SDoF and capacity because of this deficiency of the channel sounding.

TABLE I
PARAMETERS FOR THE SDOF AND CAPACITY EVALUATION.

Parameter	Symbol	Value
Tx power	P_{t}	-23.3 dBm/MHz
Temperature	T	293 K
Rx noise figure	NF	10 dB

IV. CAPACITY EVALUATION

A. Method

The intrinsic channel capacity of each link at different radio frequencies is estimated from (5). The mode coupling vector $\boldsymbol{m}$ was obtained by (3) together with the parameters of propagation paths (2) estimated from the measurements as detailed in Section III. The dimension of $\boldsymbol{m}$ was determined by the Rx antenna aperture size in (1) with $\epsilon = 0$; 100 small-scale realizations of $\boldsymbol{m}$ were obtained by allocating a random phase to the amplitude of propagation paths $\boldsymbol{\alpha}$. The ensemble averaging in (4) was taken over the 100 realizations. The noise level at the Rx was set such that $\sigma^2 = kTB \cdot 10^{\frac{NF}{10}}$, where k is the Boltzmann constant, T is the absolute temperature of the environment and NF is the noise figure of the Rx. Link parameter values for the capacity estimation are as summarized in Table I. The bandwidth and the Tx power is set assuming a single subcarrier of the orthogonal frequency division multiplexing signaling in the 802.11ad-2012 standard with the total Tx power of 10 dBm over 2.16 GHz bandwidth [10]. An ideal circular antenna aperture with a half-gain beamwidth of 10°, which is the Rx angular resolution of our channel sounding, has 2.95λ radius, $27.3\lambda^2$ size and 25.4 dB gain. Assuming that this ideal circular aperture is installed at the Rx for the capacity estimation, the dynamic range of the link simulation becomes 114.6 dB. Since the dynamic range of the channel sounding at the three frequencies are greater than that of link simulations as shown in Section III, the link simulations allow a fair comparison of the intrinsic channel capacity at the three radio frequencies in a consistent manner with our channel sounding. Furthermore, it must be noted that the capacity simulation with larger Rx aperture than $27.3\lambda^2$ does not provide sound estimates because the corresponding azimuth angular resolution becomes better than that realized in the channel sounding.

B. Results and Discussion

1) Fixed electrical size of Rx aperture: Figure 3 depicts the estimated intrinsic channel capacity and the SDoF with the same *electrical* antenna aperture size at the Rx, $27.3\lambda^2$. The identical electrical size leads to the same azimuth angular resolution and the gain at the Rx, i.e., 10° and 25.4 dB in this case, and corresponds to 109.4, 31.4 and 6.6 cm^2 in physical size at 15, 28 and 61 GHz. Given the same Tx power and

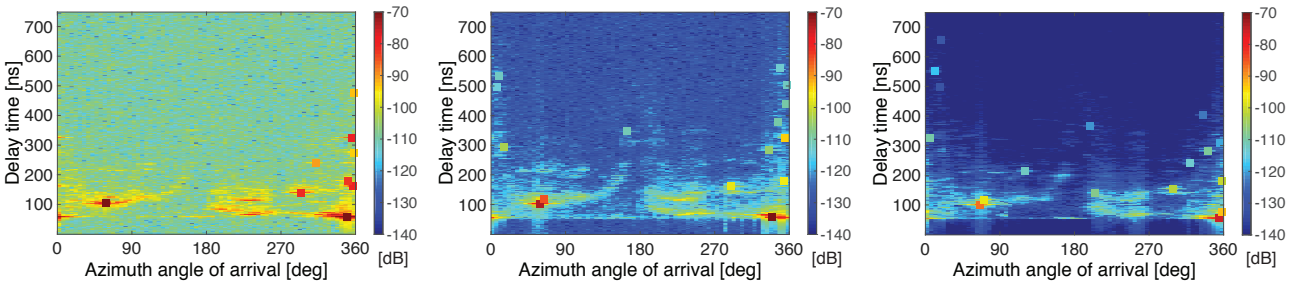

(a) (b) (c)

Fig. 2. PADPs for Tx3 measured at (a) 15, (b) 28 and (c) 61 GHz.

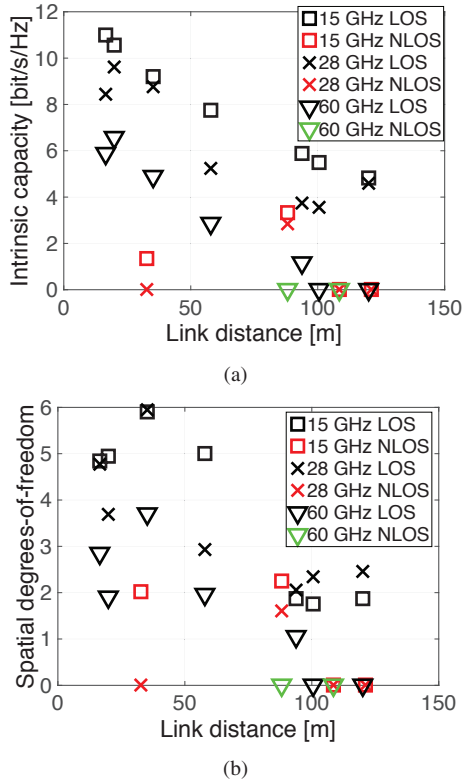

(a) (b)

Fig. 3. (a) Intrinsic channel capacity and (b) SDoF when the Rx antenna aperture is $27.3\lambda^2$.

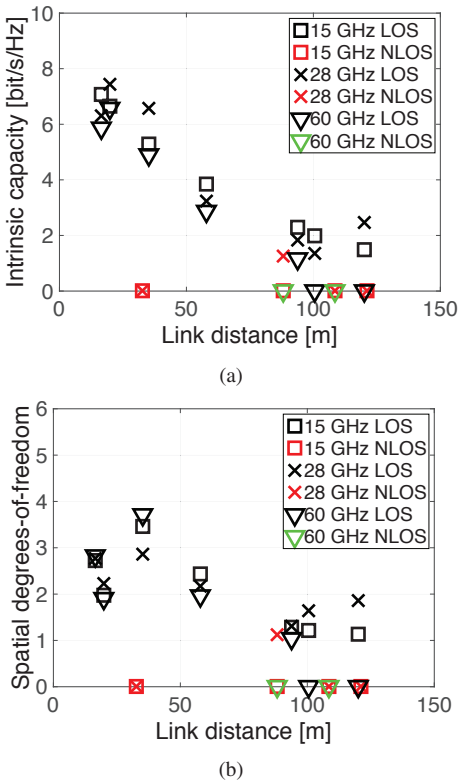

(a) (b)

Fig. 4. (a) Intrinsic channel capacity and (b) SDoF when the Rx antenna aperture is 6.6cm^2, i.e., $27.3\lambda^2$ at 60 GHz.

the noise level in the link simulations, the figure shows the extent of multipath richness within a signal dynamic range. The capacity in Fig. 3(a) indicates an intuitive trend that lower frequency radio channels give greater capacity due to the same Tx and Rx antenna gains; 61 GHz channels suffer from a low signal-to-noise ratio (SNR) in NLOS cases and in LOS links greater than 100 m, where the observed propagation paths are very few and weak. Figure 3(b) however shows a counter-intuitive trend that 28 GHz channels have the same level of SDoF as 15 GHz in many links. This may be in line with a finding in [4] that the Rx angular spread at 28 GHz is greatest among the three frequencies in many links, possibly because of absence of cars in the street that block specular reflections from building walls at 15 and 60 GHz in LOS links. It is worthwhile to note that the similar level of SDoF at 15 and 28 GHz did not lead to a comparable capacity in Fig. 3(a) because the eigenchannels are weaker at 28 GHz than 15 GHz; the number of eigenchannels above the Rx noise level is identical to the SDoF as defined in (6).

2) Fixed physical size of Rx aperture: Figures 4 and 5 illustrate the estimated intrinsic channel capacity and SDoF with the same *physical* aperture size at the Rx; Fig. 4 shows them with 6.6 cm^2 and Fig. 5 for 31.4 cm^2. These two sizes correspond to $27.3\lambda^2$ that achieve 10° azimuth angular resolution at 61 and 28 GHz with the idealistic Rx circular aperture. Figure 5 does not include the capacity estimates at

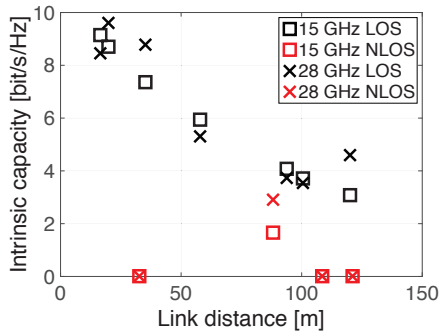

(a)

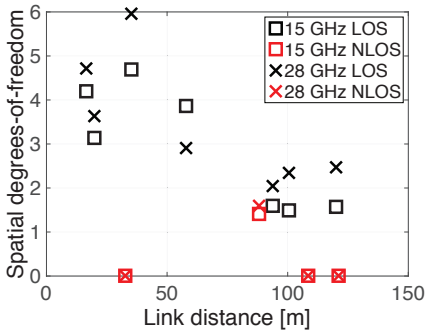

(b)

Fig. 5. (a) Intrinsic channel capacity and (b) SDoF when the Rx antenna aperture is 31.4cm^2, i.e., $27.3\lambda^2$ at 28 GHz.

61 GHz since the aperture size at the frequency is greater than $27.3\lambda^2$, which we specified in Section IV-A as the upper limit of the aperture size that can be evaluated faithfully with our the channel sounding. Figure 4(a) show that channels at the three frequencies provide almost comparable levels of capacity when the link distance is less than 100 m and is LOS. The capacity of a link with greater separation than 100 m is outage at 61 GHz because of the very few and weak multipaths observed in these links. Almost the same trend was observed in the SDoF according to Fig. 4(b); they are comparable at the three frequencies mostly, except for longer Tx-Rx separation distances than 100 m where 61 GHz links have zero SDoF where all the eigenchannels are below the noise floor even after eigenbeamforming.

The comparison of the capacity and SDoF with $31.4\ \text{cm}^2$ Rx aperture size is shown in Figure 5. The figure brings an important finding that 28 GHz channels have almost comparable performance to 15 GHz. Even though there are less multipaths at 28 GHz than 15 GHz as discussed in IV-B1 based on Fig. 3(b), the increased gain focusing and finer angular resolution of the Rx aperture normalizes the attainable channel capacity. Figure 5(b) shows that the SDoF is indeed greater at 28 GHz than 15 GHz with the same physical size of the Rx aperture.

V. Concluding Remarks

This paper reported attainable capacity and SDoF of 15, 28 and 61 GHz channels based on measurements in a same street canyon. The analysis showed that the inherent multipath richness of the channel, which is indicated as the SDoF for a given *electrical* antenna aperture size leading to the same angular resolution of the channel, decreases as the frequency increases. However, the channels at three frequencies show almost comparable capacity for a given *physical* aperture size in our LOS conditions. The 60 GHz LOS channels with greater Tx-Rx separation than 100 m suffer from a low SNR due to a small number of multipaths that are very weak. Finally, it is worth pointing out that the channels at the three frequencies are equally powerless in the studied NLOS conditions with the given transmit power, and hence we saw capacity outage mostly. It is essential to extend this study to other environments to observe if the findings from the present analysis hold there too.

Acknowledgement

The research leading to these results received funding from the European Commission H2020 programme under grant agreement in °671650 (5G mmMAGIC project). The authors also would like to thank the financial support of the Academy of Finland through the WiFiUS project "Device-to-Device Communications at Millimeter-Wave Frequencies", decision number 284709. Finally, support of Mr. Jan Jarvelainen, Mr. Reza Naderpour and Mr. Abbas Manavi Nezhad from Aalto University during channel measurements is acknowledged.

References

[1] W. Roh, J.-Y. Seol, J.-H. Park, B. Lee, J. Lee, Y. Kim, J. Cho, K. Cheun, and F. Aryanfar, "Millimeter-wave beamforming as an enabling technology for 5G cellular communications: theoretical feasibility and prototype results," *IEEE Commun. Mag.*, vol. 52, pp. 106–113, Feb. 2014.

[2] M.-R. Akdeniz, Y. Liu, M.-K. Samimi, S. Sun, S. Rangan, T.-S. Rappaport, and E. Erkip, "Millimeter wave channel modeling and cellular capacity evaluation," *IEEE J. Sel. A. Commun.*, vol. 6, no. 6, pp. 1164–1179, Sep. 2014.

[3] A.-S.-Y. Poon, R.-W. Brodersen, and D.-N.-C. Tse, "Degrees of freedom in multiple-antenna channels: a signal space approach," *IEEE Trans. Inf. Theory*, vol. 51, no. 2, pp. 523–536, Feb. 2005.

[4] R. Naderpour, J. Vehmas, S. Nguyen, J. Jarvelainen, and K. Haneda, "Spatio-temporal channel sounding in a street canyon at 15, 28 and 60 GHz," in *Proc. 27th Int. Symp. Personal Indoor Mobile Radio Commun. (PIMRC '16)*, Valencia, Spain, Sep. 2016.

[5] K. Haneda, C. Gustafson, and S. Wyne, "60 GHz spatial radio transmission: Multiplexing or beamforming?" *IEEE Trans. Ant. Prop.*, vol. 61, no. 11, pp. 5735–5743, Nov. 2013.

[6] J.-W. Wallace and M.-A. Jensen, "Intrinsic capacity of the MIMO wireless channel," in *Proc. IEEE 56th Veh. Technol. Conf. (VTC 2002-Fall)*, vol. 2, 2002, pp. 701–705.

[7] J.-E. Hansen, *Spherical near-field antenna measurement*. IEE Electromagnetic waves series 26, Peter Peregrinus, London, UK, 1998.

[8] K. Haneda, A. Khatun, M. Dashti, T. Laitinen, V.-M. Kolmonen, J. Takada, and P. Vainikainen, "Measurement-based analysis of a spatial degrees-of-freedom in propagation channels," *IEEE Trans. Ant. Prop.*, vol. 61, no. 2, pp. 890–900, Feb. 2013.

[9] K. Haneda, S. Nguyen, J. Jarvelainen, and J. Putkonen, "Estimating the omni-directional pathloss from directional channel sounding," in *Proc. 10th European Conf. Ant. Prop. (EuCAP2016)*, Davos, Switzerland, Apr. 2016.

[10] IEEE, "Part 11: wireless LAN Medium Access Control and Physical Layer Specifications Amendment 3: Enhancements for Very High Throughput in the 60 GHz Band," IEEE Standard 802.11ad-2012, 2012.